Sea surface exchanges of momentum, heat, and freshwater determined by satellite remote sensing

Lisan Yu

Department of Physical Oceanography
Woods Hole Oceanographic Institution
Woods Hole, MA 02543, USA

Mailing address:

Department of Physical Oceanography, MS#21
Woods Hole Oceanographic Institution
360 Woods Hole Road
Woods Hole, MA 02543, USA

Phone: 1 508 289 2504;
Fax: 1 508 457 2181;
Email: lyu@whoi.edu

In: J. Steele, S. Thorpe, and K. Turekian (eds.),
Encyclopedia of Ocean Sciences, First Online Update
Academic Press, London, UK.

Accepted.
October, 2007

Keywords

El Niño – Southern Oscillation
Evaporation
Freshwater flux
Latent heat flux
Longwave radiation
Satellite remote sensing
Sea surface flux estimation
Sensible heat flux
Shortwave radiation
Surface wind fields

Sea surface exchanges of momentum, heat, and freshwater determined by satellite remote sensing

Synopsis

The ocean and the atmosphere communicate through the interfacial exchanges of physical, chemical, and biological properties. The amount of sea-surface exchange is called sea-surface flux. This paper focuses on air-sea physical fluxes, which include momentum, heat, and freshwater. The surface fluxes are characterized by large spatial and temporal variability, and play an important role in not only the mean atmospheric and oceanic circulation but also the coupled climate fluctuations such as the El Niño – Southern Oscillation (ENSO). The satellite sensor systems developed in the past two decades provide unprecedented global observations of geophysical parameters in the lower atmosphere and upper oceans, thus providing opportunity to estimate near real-time sea-surface fluxes with unprecedented accuracy and resolution. This article reviews the methods of deriving sea-surface momentum, heat, and freshwater fluxes from space observations, and reviews the types of satellite measurements required by the methods, and the types of spaceborne sensors from which those measurements can be retrieved. This article also provides an example of synergizing various satellite sea surface products to study the complex scale-interactions between the atmosphere and ocean in the 1997-98 ENSO.

Introduction

The ocean and the atmosphere communicate through the interfacial exchanges of heat, freshwater, and momentum. While the transfer of the momentum from the atmosphere to the ocean by wind stress is the most important forcing of the ocean circulation, the heat and water exchanges affect the horizontal and vertical temperature gradients of the lower atmosphere and the upper ocean that, in turn, modify wind and ocean currents and maintain the equilibrium of the climate system. The sea surface exchanges are the fundamental processes of the coupled atmosphere-ocean system. An accurate knowledge of the flux variability is critical to our understanding and prediction of the changes of global weather and climate.

The heat exchanges include four processes: the shortwave radiation (Q_{SW}) from the sun, the outgoing longwave radiation (Q_{LW}) from the sea surface, the sensible heat transfer (Q_{SH}) resulting from air-sea temperature differences, and the latent heat transfer (Q_{LH}) carried by evaporation of sea surface water. Evaporation releases both energy and water vapor to the atmosphere, and thus, links the global energy cycle to the global water cycle. The oceans are the key element of the water cycle, because the oceans contain 96 percent of the Earth's water, experience 86 percent of planetary evaporation, and receive 78 percent of planetary precipitation.

The amount of air-sea exchange is called sea-surface (or air-sea) flux. Direct flux measurements by ships and buoys are very limited. Our present knowledge of the global sea surface flux distribution stems primarily from bulk parameterizations of the fluxes as functions of surface meteorological variables that can be more easily measured (e.g., wind speed, temperature, humidity, cloud cover, precipitation, etc). Before the advent of satellite remote sensing, marine surface weather reports collected from Voluntary Observing Ships (VOS) have been the backborne for constructing the climatological state of the global flux fields. Over the past two decades, satellite remote sensing has become a mature technology for remotely sensing key air-sea variables. With continuous global spatial coverage, consistent quality, and high temporal sampling, satellite measurements not only allow the construction of air-sea fluxes at near-real time with unprecedented quality but most importantly, also offer the unique opportunity to view the global ocean synoptically as an entity.

Flux estimation using satellite observations

Sea surface wind stress

The Seasat-A satellite scatterometer, launched in June 1978, was the first mission to demonstrate that ocean surface wind vectors (both speed and direction) could be remotely sensed by active radar backscatter from measuring surface roughness. Scatterometer detects the loss of intensity of transmitted microwave energy from that returned by the ocean surface. Microwaves are scattered by wind-driven capillary waves on the ocean surface, and the fraction of energy returned to the satellite (backscatter) depends on both the magnitude of the wind stress and the wind direction relative to the direction of the radar beam (azimuth angle). By using a transfer function or an empirical algorithm, the backscatter measurements are converted to wind vectors. It is true that scatterometers measure the effects of small-scale roughness caused by surface stress; but the retrieval algorithms produce surface wind, not

wind stress, because there are no adequate surface stress "ground-truths" to calibrate the algorithms. The wind retrievals are calibrated to the equivalent neutral-stability wind at a reference height of 10m above the local-mean sea surface. This is the 10-m wind that would be associated with the observed surface stress if the atmospheric boundary layer were neutrally stratified. The 10-m equivalent neutral wind speeds differ from the 10-m wind speeds measured by anemometers; and these differences are a function of atmospheric stratification and are normally in the order of 0.2 ms^{-1}. To compute surface wind stress, τ, the conventional bulk formulation is then employed,

$$\tau = (\tau_x, \tau_y) = \rho\, c_d W(u, v) \qquad (1)$$

where τ_x and τ_y, are the zonal and meridional components of the wind stress; W, u and v are the scatterometer-estimated wind speed at 10m and its zonal component (eastward) and meridional component (northward), respectively. The density of surface air is given by ρ and is equal approximately to 1.225 kg m^{-3}, and c_d is a neutral 10m drag coefficient.

Scatterometer instruments are typically deployed on sun-synchronous near-polar-orbiting satellites that pass over the equator at approximately the same local times each day. These satellites orbit at an altitude of approximately 800 km and are commonly known as Polar Orbiting Environmental Satellites (POES). There have been six scatterometer sensors aboard POES since the early 1990s. Major characteristics of all scatterometers are summarized in Table 1. The first European Remote Sensing (ERS-1) was launched by the European Space Agency (ESA) in August 1991. An identical instrument aboard the successor ERS-2 became operational in 1995, but failed in 2001. In August 1996, the National Aeronautics and Space Administration (NASA) began a joint mission with the National Space Development Agency (NASDA) of Japan to maintain continuous scatterometer missions beyond ERS satellites. The joint effort led to the launch of the NASA scatterometer (NSCAT) aboard the first Japanese Advanced Earth Observing Satellite (ADEOS-I). The ERA scatterometers differ from the NASA scatterometers in that the former operate on the C-band (~ 5 GHz), while the latter use the Ku-band (~ 14 GHz). For radio-frequency band, rain attenuation increases as the signal frequency increases. Compared to C-band satellites, the higher frequencies of Ku-band are more vulnerable to signal quality problems caused by rainfall. However, Ku-band satellites have the advantage of being more sensitive to wind variation at low winds and covering more area.

Table 1

Rain has three effects on backscatter measurements. It attenuates the radar signal, introduces volume scattering, and changes the properties of the sea surface and consequently the properties of microwave signals scattered from the sea surface. When the backscatter from the sea surface is low, the additional volume scattering from rain will lead to an overestimation of the low wind speed actually present. Conversely, when the backscatter is high, attenuation by rain will reduce the signal causing an underestimation of the wind speed.

Under rain-free conditions, scatterometer-derived wind estimates are accurate within 1ms^{-1} for speed and 20 degrees for direction. For low (less than 3ms^{-1}) and high winds (greater than 20ms^{-1}), the uncertainties are generally larger. Most problems with low wind retrievals are due to the weak backscatter signal that is easily confounded by noise. The low signal/noise ratio complicates the ambiguity removal processing in selecting the best wind vector from the set of ambiguous wind vectors. Ambiguity removal is over 99% effective for wind speed 8 ms^{-1} and higher. Extreme high winds are mostly associated with storm events. Scatterometer-derived high winds are found to be underestimated due largely to deficiencies

of the empirical scatterometer algorithms. These algorithms are calibrated against a subset of ocean buoys – although the buoy winds are accurate and serve as surface wind truth, few of them have high wind observations.

NSCAT worked flawlessly, but the spacecraft (ADEOS-I) that hosted it demised prematurely in June 1997 after only nine months of operation. A replacement mission called QuikSCAT was rapidly developed and launched in July 1999. To date, QuikSCAT remains in operation, far outlasting the expected 2-3 year mission life expectancy. QuikSCAT carries a Ku-band scatterometer named SeaWinds, which has accuracy characteristics similar to NSCAT but with improved coverage. The instrument measures vector winds over a swath of 1800 km with a nominal spatial resolution of 25 km. The improved sampling size allows approximately 93% of the ocean surface to be sampled on a daily basis as opposed to two days by NSCAT and four days by the ERS instruments. A second similar version SeaWinds instrument was placed on the ADEOS-II mission in December 2002. However, after only a few months of operation, it followed the unfortunate path of NSCAT and failed in October 2003 due – once again – to power loss.

The Advanced Scatterometer (ASCAT) launched by ESA/EUMETSAT in March 2007 is the most recent satellite designed primarily for the global measurement of sea-surface wind vectors. ASCAT is flown on the first of three METOP satellites. Each METOP has a design lifetime of 5 years and thus, with overlap, the series has a planned duration of 14 years. ASCAT is similar to ERS-1/2 in configuration except that it has increased coverage, with two 500-km swaths (one on each side of the spacecraft nadir track).

The data collected by scatterometers on various missions have constituted a record of ocean vector winds for more than a decade long starting in August 1992. These satellite winds provide synoptic global view from the vantage point of space, and provide excellent coverage in regions, such as the southern oceans, that are poorly sampled by the conventional observing network. Scatterometers have shown to be the only means of delivering observations at adequate ranges of temporal and spatial scales and at adequate accuracy for understanding ocean-atmosphere interactions and global climate changes, and for improving climate predictions on synoptic, seasonal, and interannual timescales.

Surface radiative fluxes

Direct estimates of surface shortwave and longwave fluxes that resolve synoptic-to-regional variability over the globe have only become possible with the advent of satellite in the past two decades. The surface radiation is a strong function of clouds. Low, thick clouds reflect large amounts of solar radiation and tend to cool the surface of the Earth. High, thin clouds transmit incoming solar radiation, but at the same time, they absorb the outgoing longwave radiation emitted by the Earth and radiate it back downward. The portion of radiation, acting as an effective “greenhouse gas”, adds to the shortwave energy from the sun and causes an additional warming of the surface of the Earth. For a given cloud, its effect on the surface radiation depends on several factors, including the cloud's altitude, size, and the particles that form the cloud. At present, the radiative heat fluxes at the earth's surface are estimated from top-of the-atmosphere (TOA) shortwave (SW) and longwave (LW) radiance measurements in conjunction with radiative transfer models.

Satellite radiance measurements are provided by two types of radiometers: scanning radiometers, and nonscanning wide field-of-view radiometers. Scanning radiometers view radiance from a single direction and must estimate the hemispheric emission or reflection. Nonscanning radiometers view the entire hemisphere of radiation with a roughly 1000-km field of view. The first flight of an Earth Radiation Budget Experiment (ERBE) instrument in 1984 included both a scanning radiometer and a set of nonscanning radiometers. These instruments obtain good measurements of TOA radiative variables including insolation, albedo, and absorbed radiation. To estimate surface radiation fluxes, however, more accurate information on clouds is needed.

To determine the physical properties of clouds from satellite measurements, the International Satellite Cloud Climatology Project (ISCCP) was established in 1983. ISCCP pioneered the cross-calibration, analysis and merger of measurements from the international constellation of operational weather satellites. Using geostationary satellite measurements with polar-orbiter measurements as supplemental when there are no geostationary measurements, the ISCCP cloud retrieval algorithm includes the conversion of radiance measurements to cloud scenes and the inference of cloud properties from the radiance values. Radiance thresholds are applied to obtain cloud fractions for low, middle, and high clouds based on radiance computed from models using observed temperature and climatological lapse rates.

In addition to the global cloud analysis, ISCCP also produces radiative fluxes (up, down, net) at the Earth's surface that parallels the effort undertaken by the Global Energy and Water Cycle Experiment – Surface Radiation Budget (GEWEX-SRB) project. The two projects use the same ISCCP cloud information but different ancillary data sources and different radiative transfer codes. They both compute the radiation fluxes for clear and cloudy skies to estimate the cloud effect on radiative energy transfer. Both have a 3-hour resolution, but ISCCP fluxes are produced on a 280 km equal-area (EQ) global grid while GEWEX-SRB fluxes are on a 1×1-degree global grid. The two sets of fluxes have reasonable agreement with each other on the long-term mean basis, as suggested by the comparison of the global annual surface radiation budget in Table 2. The total net radiation differs by about 5Wm^{-2} due mostly to the SW component. However, when compared with ground-based observations, the uncertainty of these fluxes is about 10-15 Wm^{-2}. The main cause is the uncertainties in surface and near-surface atmospheric properties such as surface skin temperature, surface air and near-surface-layer temperatures and humidity, aerosols, etc. Further improvement requires improved retrievals of these properties.

Table 2

In the late 1990s, the Clouds and the Earth's Radiant Energy System (CERES) experiment was developed by NASA's Earth Observing System (EOS) not only to measure TOA radiative fluxes but also to determine radiative fluxes within the atmosphere and at the surface, by using simultaneous measurements of complete cloud properties from other EOS instruments such as the Moderate-Resolution Imaging Spectroradiometer (MODEIS). CERES instruments were launched aboard the Tropical Rainfall Measuring Mission (TRMM) in November 1997, on the EOS Terra satellite in December 1999, and on the EOS Aqua spacecraft in 2002. There is no doubt that the EOS era satellite observations will lead to great improvement in estimating cloud properties and surface radiation budget with sufficient simultaneity and accuracy.

Sea surface turbulent heat fluxes

Latent and sensible heat fluxes are the primary mechanism by which the ocean transfers much of the absorbed solar radiation back to the atmosphere. The two fluxes cannot be directly observed by space sensors, but can be estimated from wind speed and sea-air humidity/temperature differences using the following bulk parameterizations:

$$Q_{LH} = \rho\, L_e c_e W(q_s - q_a) \qquad (2)$$
$$Q_{SH} = \rho\, c_p c_h W(T_s - T_a) \qquad (3)$$

where L_e is the latent heat of vaporization and is a function of SST (T_s) expressed as $L_e = (2.501 - 0.00237\times T_s)\times 1.0^6$. c_p is the specific heat capacity of air at constant pressure, c_e and c_h are the stability and height dependent turbulent exchange coefficients for latent and sensible heat respectively. T_a/q_a are the temperature/specific-humidity at a reference height of 2m above the sea surface. q_s is the saturation humidity at T_s, and is multiplied by 0.98 to take into account the reduction in vapor pressure caused by salt water.

The two variables, T_s and W, in Eqs. (2)–(3) are retrieved from satellites, and so q_s is known. The remote sensing of T_s is based on techniques by which spaceborne infrared and microwave radiometers detect thermally emitted radiation from the ocean surface. Infrared radiometers like the five-channel Advanced Very High Resolution Radiometer (AVHRR) utilize the wavelength bands at 3.5-4 μm and 10-12 μm that have a high transmission of the cloud-free atmosphere. The disadvantage is that clouds are opaque to infrared radiation and can effectively mask radiation from the ocean surface, and this affects the temporal resolution. Although the AVHRR satellite orbits the Earth 14 times each day from 833 km above its surface and each pass of the satellite provides a 2399-km-wide swath, it usually takes one or two weeks, depending on the actual cloud coverage, to obtain a complete global coverage. Clouds, on the other hand, have little effect on the microwave radiometers so that microwave T_s retrievals can be made under complete cloud cover except for raining conditions. The TRMM microwave imager (TMI) launched in 1997 has a full suite of channels ranging from 10.7 to 85 GHz and was the first satellite sensor capable of accurately measuring SST through clouds. The low-inclination equitorial orbit, however, limits the TMI's coverage only up to approximately 38-deg latitude. Following TMI, the first polar orbiting microwave radiometer capable of measuring global through-cloud SST was made possible by the NASDA's Advanced Microwave Scanning Radiometer (AMSR) flown aboard the NASA's EOS Aqua mission in 2002.

While SST can be measured in both infrared and microwave regions, the near-surface wind speed can only be retrieved in the microwave region. The reason is that the emissivity of the ocean's surface at wavelengths of around 11 μm is so high that it is not sensitive to changes in the wind-induced sea surface roughness or humidity fluctuations in the lower atmosphere. Microwave wind speed retrievals are provided by the Special Sensor Microwave/Imager (SSM/I) that has been flown on a series of polar-orbiting operational spacecrafts of the Defense Meteorological Space Program (DMSP) since July 1987. SSM/I has a wide swath (~1400km) and a coverage of 82% of the earth's surface within one day. But unlike scatterometers, SSM/I is a passive microwave sensor and cannot provide information on the wind direction. This is not a problem for the computation in Eqs.(2)–(3) that requires only wind speed observations. In fact, the high space-time resolution and good global coverage of SSM/I has made it serving as a primary database for computing the climate mean and variability of the oceanic latent and sensible heat fluxes over the past nearly 20-year

period. At present, wind speed measurements with good accuracy are also available from several NASA satellite platforms, including TMI and AMSR.

The most difficult problem for the satellite-based flux estimation is the retrieval of the air humidity and temperature, q_a and T_a, at a level of several meters above the surface. This problem is inherent to all spaceborne passive radiometers, because the measured radiation emanates from relatively thick atmospheric layers rather than from single levels. One common practice to extract satellite q_a is to relate q_a to the observed column integrated water vapor (IWV, also referred to as the total precipitable water) from SSM/I. Using IWV as a proxy for q_a is based on several observational findings that on monthly timescales the vertical distribution of water vapor is coherent throughout the entire atmospheric column. The approach, however, produces large systematic biases of over 2 g kg^{-1} in the Tropics, as well as in the mid and high latitudes during summertime. This is caused by the effect of the water vapor convergence that is difficult to assess in regions where the surface air is nearly saturated but the total integrated water vapor is small. Under such situations, the integrated water vapor cannot reflect the actual vertical and horizontal humidity variations in the atmosphere. Various remedies have been proposed to improve the q_a–IWV relation and to make it applicable on synoptic and shorter timescales. There are methods of including additional geophysical variables, replacing IWV with the IWV in the lower 500 m of the planetary layer, and/or using Empirical Orthogonal Functions (EOFs). Although overall improvements were achieved, the accuracy remains poor due to the lack of detailed information on the atmospheric humidity profiles.

Retrieving T_a from satellite observations is even more challenging. Unlike humidity, there is no coherent vertical structure of temperature in the atmosphere. Satellite temperature sounding radiometers offer little help, as they generally are designed for retrieval in broad vertical layers. The sounder's low information content in the lower atmosphere does not enable the retrieval of near-surface air temperature with sufficient accuracy. Different methods have been tested to derive T_a from the inferred q_a, but all showed limited success. Because of the difficulties in determining q_a and T_a, latent and sensible fluxes estimated from satellite measurements have large uncertainties.

Three methods have been tested for obtaining better q_a and T_a to improve the estimates of latent and sensible fluxes. The first approach is to enhance the information on the temperature and moisture in the lower troposphere. This is achieved by combining SSM/I data with additional microwave sounder data that come from the instruments like the Advanced Microwave Sounding Unit (AMSU-A) and Microwave humidity sounder (MHS) flown aboard the National Oceanic and Atmospheric Administration (NOAA) polar orbiting satellites, and the Special Sensor Microwave Temperature Sounder (SSM/T) and (SSM/T-2) on the DMSP satellites. Although the sounders do not directly provide shallow surface measurements, detailed profile information provided by the sounders can help to remove variability in total column measurements not associated with the surface. The second approach is to capitalize the progress made in numerical weather prediction models that assimilate sounder observations into the physically based system. The q_a and T_a estimates from the models contain less ambiguity associated with the vertical integration and large spatial averaging of the various parameters, though they are subject to systematic bias due to model's sub-grid parameterizations. The third approach is to obtain a better estimation of q_a and T_a through an optimal combination of satellite retrievals with the model outputs, which has been experimented by the Objectively Analyzed air-sea Fluxes (OAFlux) project at the

Woods Hole Oceanographic Institution (WHOI). The effort has led to improved daily estimates of global air-sea latent and sensible fluxes.

Freshwater flux

The freshwater flux is the difference between precipitation (rain) and evaporation. Evaporation releases both water vapor and latent heat to the atmosphere. Once latent heat fluxes are estimated, the sea surface evaporation (E) can be computed using the following relation:

$$E = Q_{LH}/\rho_w L_e \qquad (4)$$

where Q_{LH} denotes latent heat flux and ρ_w is the density of sea water.

Spaceborne sensors cannot directly observe the actual precipitation reaching the earth's surface, but they can measure other variables that may be highly correlated with surface rainfall. These include variations in infrared and microwave brightness temperatures, as well as visible and near-infrared albedo. Infrared techniques are based on the premise that rainfall at the surface is related to cloud top properties observed from space. Visible/infrared observations supplement the infrared imagery with visible imagery during daytime to help eliminate thin cirrus clouds, which are cold in the infrared imagery and are sometimes misinterpreted as raining using infrared data alone. Visible/infrared sensors have the advantage of providing good space and time sampling, but have difficulty capturing the rain from warm-topped clouds. By comparison, microwave estimates are more physically based and more accurate although time and space resolutions are not as good. The principle of MW techniques is that rainfall at the surface is related to microwave emission from rain drops (low frequency channels) and microwave scattering from ice (high frequency channels). While the primary visible/infrared data sources are the operational geostationary satellites, microwave observations are available from SSM/I, the NOAA AMSU-B, and the TRMM spacecrafts.

TRMM opened up a new era of estimating not only surface rainfall but also rain profiles. TRMM is equipped with the first spaceborne precipitation radar (PR) along with a microwave radiometer (TMI) and a visible/infrared radiometer (VIRS). Coincident measurements from the three sensors are complementary. PR provides detailed vertical rain profiles across a 215 km wide strip. TMI (a 5-frequency conical scanning radiometer), though has less vertical and horizontal fidelity in rain resolving capability, features a swath width of 760 km. The VIRS on TRMM adds cloud-top temperatures and structures to complement the description of the two microwave sensors. While direct precipitation information from VIRS is less reliable than that obtained by the microwave sensors, VIRS serves an important role as a bridge between the high quality but infrequent observations from TMI and PR with the more available data and longer time series data available from the geostationary visible/infrared satellite platforms.

The TRMM satellite focuses on the rain variability over the tropical and sub-tropical regions due to the low inclination. An improved instrument, AMSR, has extended TRMM rainfall measurements to higher latitudes. AMSR is currently aboard the Aqua satellite and is planned by the Global Precipitation Measurement (GPM) mission to be launched in 2009. Combining rainfall estimates from visible/infrared with microwave measurements is being undertaken by the Global Climatology Project (GPCP) to produce global precipitation analyses from 1979 and continuing.

Summary and applications

The satellite sensor systems developed in the past two decades have provided unprecedented observations of geophysical parameters in the lower atmosphere and upper oceans. The combination of measurements from multiple satellite platforms has demonstrated the capability of estimating sea-surface heat, freshwater, and momentum fluxes with sufficient accuracy and resolution. These air-sea flux datasets, together with satellite retrievals of ocean surface topography, temperature, and salinity (Figure 1), establish a complete satellite-based observational infrastructure to fully monitoring the ocean's response to the changes in air-sea physical forcing.

Figure 1

Atmosphere and the ocean are nonlinear turbulent fluids, and their interactions are nonlinear scale-dependent, with processes at one scale affecting processes at other scales. The synergy of various satellite-based products makes it especially advantageous to study the complex scale interactions between the atmosphere and the ocean. One clear example is the satellite monitoring of the development of the El Niño-Southern Oscillation (ENSO) in 1997-98. ENSO is the largest source of interannual variability in the global climate system. The phenomenon is characterized by the appearance of extensive warm surface water over the central and eastern tropical Pacific Ocean at a frequency roughly 3-7 years. The 1997-98 El Niño was one of the most severe events experienced during the twentieth century. During the peak of the event in December 1997 (Figure 2), the SST in the eastern equatorial Pacific was more than 5°C above normal, and the warming was accompanied by excessive precipitation and large net heat transfer from the ocean to the atmosphere.

Figure 2

The 1997-98 event was also the best observed thanks largely to the expanded satellite observing capability. One of the major observational findings was the role of synoptic westerly wind bursts (WWB) in the onset of El Niño. Figure 3 presents the evolution of zonal wind from NSCAT scatterometer combined with SSM/I derived wind product, sea surface height (SSH) from TOPEX altimetry, and SST from AVHRR imagery in 1996-1998. The appearance of the anomalous warming in the eastern basin in February 1997 coincided with the arrival of the downwelling Kelvin waves generated by the WWB of December 1996 in the western Pacific. A series of subsequent WWB-induced Kelvin waves further enhanced the eastern warming, and fueled the El Niño development. The positive feedback between synoptic WWB and the interannual SST warming in making an El Niño is clearly indicated by satellite observations. On the other hand, the synoptic WWB events were the result of the development of equatorial twin cyclones under the influence of northerly cold surges from East Asia/Western North Pacific. NSCAT made the first complete recording of the compelling connection between near-equatorial wind events and midlatitude atmospheric transient forcing.

Figure 3

Clearly, the synergy of various satellite products offers consistent global patterns that facilitate the mapping of the correlations between various processes and the construction of the teleconnection pattern between weather and climate anomalies in one region and those in another. The satellite observing system will complement the in situ ground observations and play an increasingly important role in understanding the cause of global climate changes and in improving the model skills on predicting weather and climate variability.

Further Reading

Adler, R. F., Huffman, G. J., Chang, A., Ferraro, R., Xie, P., et al., (2003). The Version 2 Global Precipitation Climatology Project (GPCP) monthly precipitation analysis (1979-Present). *Journal of Hydrometeorology*, **4**, 1147-1167.

Atlas R., Hoffman, R. N., Bloom, S. C., Jusem, J. C., and Ardizzone, J., (1996). A multiyear global surface wind velocity dataset using SSM/I wind observations. *Bulletin of the American Meteorological Society*, **77**, 869–882.

Bentamy, A, Katsaros, K. B., Mestas-Nuñez, A. M., Drennan, W. M., Forde, E. B., et al. (2003). Satellite estimates of wind speed and latent heat flux over the global oceans. *Journal of Climate*, **16**, 637–656.

Chou S.-H., Nelkin, E., Ardizzone, J., Atlas, R. M., and Shie, C.-L. (2003). Surface turbulent heat and momentum fluxes over global oceans based on the Goddard satellite retrievals, version 2 (GSSTF2). *Journal of Climate*, **16**, 3256–3273.

Gupta S. K., Ritchey, N. A., Wilber, A. C., Whitlock, C. H., Gibson, G. G., and Stackhouse Jr., P. W., (1999). A climatology of surface radiation budget derived from satellite data. *Journal of Climate*, **12**, 2691–2710.

Liu, W.T., and Katsaros, K. B. (2001). Air-Sea Flux from Satellite Data. In Siedler,G., Church, J., & Gould, J. (eds) *Ocean Circulation and Climate*. pp173-179. New York: Academic Press.

Kubota M., Iwasaka, N., Kizu, S., Konda, M., and Kutsuwada, K. (2002). Japanese Ocean Flux Data Sets with Use of Remote Sensing Observations (J-OFURO). *Journal of Oceanography*, **58**, 213–225.

Wentz, F. J., Gentemann, C., Smith, D., and Chelton, D. (2000). Satellite measurements of sea surface temperature through clouds. *Science*, **288**, 847-850.

Yu, L., and Weller, R. A. (2007). Objectively Analyzed air-sea heat Fluxes (OAFlux) for the global oceans. *Bulletin of the American Meteorological Society*, **88**, 527-539.

Zhang, Y-C., Rossow, W. B., Lacis, A. A., Oinas, V., and Mishchenko, M. I. (2004). Calculation of radiative fluxes from the surface to top of atmosphere based on ISCCP and other global data sets: Refinements of the radiative transfer model and the input data. *Journal of Geophysical Research,* **109**, D19105, doi:10.1029/ 2003JD004457.

List of useful websites

The Global Energy and Water Cycle Experiment (GEWEX):
http://www.gewex.org/

The Global Precipitation Climatology Project:
http://precip.gsfc.nasa.gov/

The International Cloud Climatology Project:
http://isccp.giss.nasa.gov/

Measuring Ocean winds from space:
http://winds.jpl.nasa.gov

The Objectively Analyzed Air-sea Fluxes Project:
http://oaflux.whoi.edu/

The Remote Sensing Systems research company:
http://www.ssmi.com/

The SEAFLUX project:
http://www.gfdi.fsu.edu/SEAFLUX/

The Surface Radiation Budget project:
http://eosweb.larc.nasa.gov/PRODOCS/srb/table_srb.html

Table 1. Major characteristics of the spaceborne scatterometers

Scatterometer / Characteristics	SeaSat-A	ERS-1	ERS-2	NSCAT	SeaWinds on QuikSCAT	SeaWinds on ADEOS II	ASCAT
Operational Frequency	Ku-band 14.6 GHz	C-band 5.255 GHz	C-band 5.255 GHz	Ku-band 13.995 GHz	Ku-band 13.402 GHz	Ku-band 13.402 GHz	C-band 5.255 GHz
Spatial Resolution	50km × 50km with 100km spacing	50km × 50km	50km × 50km	25km × 25km	25km × 25km	25km × 6km	25km × 25km
Scan characteristics	Two sided, double 500km swaths separated by a 450km nadir gap	One sided, single 500km swath	One sided, single 500km swath	Two sided, double 600km swaths separated by a 329km nadir gap	Conical scan, one wide swath of 1800km	Conical scan, one wide swath of 1800km	Two sided, double 500km swaths separated by a 700km nadir gap
Daily Coverage	variable	41%	41%	77%	93%	93%	60%
Period In Service	Jul 1978 – Oct 1978	Aug 1991 – May 1997	May 1995 – Jan 2001	Sep 1996 – Jun 1997	Jun 1999 – current	Dec 2002 – Oct 2003	Mar 2007 – current

Table 2. Annual surface radiation budget (in Wm^{-2}) over global oceans. Uncertainty estimates are based on the standard error of monthly anomalies.

Parameter / Data 21-Year Mean 1984-2004	SW Net Downward	LW Net Downward	SW+LW Net Downward
ISCCP (Zhang et al. 2004)	173.2 ± 9.2	-46.9 ± 9.2	126.3 ± 11.0
GEWEX-SRB (Gupta et al. 2006)	167.2 ± 13.9	-46.3 ± 5.5	120.9 ± 11.9

Figure captions

Figure 1. Schematic diagram of the physical exchange processes at the air-sea interface and the upper ocean responses, with corresponding sensor names shown in red.

Figure 2. (First column) An example of the Sactterometer observations of the generation of the tropical cyclones in the western tropical Pacific under the influence of northerly cold surges from East Asia/Western North Pacific. The effect of westerly wind bursts on the development of El Niño is illustrated in the evolution of the equatorial sea level observed from TOPEX/POSEIDON altimetry and SST from AVHRR. The series of westerly wind bursts (second column, SSM/I wind analysis by Atlas et al. 1996) excited a series of downwelling Kelvin waves that propagated eastward along the equator (third column), suppressed the thermocline, and led to the sea surface warming in the eastern equatorial Pacific (fourth column).

Figure 3. Satellite derived global ocean temperature from AVHRR (top), precipitation-minus-evaporation from GPCP and WHOI OAFlux, respectively (middle), and net heat loss ($Q_{LH}+Q_{SH}+Q_{LW}-Q_{SW}$) from the ocean (bottom) during the El Niño in December 1997. The latent and sensible heat fluxes $Q_{LH}+Q_{SH}$ are provided by WHOI OAFlux, and the short- and longwave radiative fluxes are by ISCCP.

Cross-references

Air–Sea Gas Exchange, B. Jähne

El Niño Southern Oscillation (ENSO) , K. E. Trenberth

Evaporation and Humidity, K. Katsaros

Heat and momentum fluxes at the sea surface, P. K. Taylor

Heat Transport and Climate, A. M. Macdonald, M. O'Neil Baringer, and A. Ganachaud

IR Radiometers, C. J. Donlon

Satellite Altimetry, R. E. Cheney

Satellite Measurements of Salinity, G. Lagerloef

Satellite Remote Sensing Microwave Scatterometers, W. J. Plant

Satellite Remote Sensing of Sea Surface Temperatures, P. J. Minnett

Satellite Oceanography, History and Introductory Concepts, S. Wilson, J. R. Apelb, and E. J. Lindstrom

Upper Ocean Heat and Freshwater Budgets, H. Wijesekera and T. J. Boyd

Wind and Buoyancy-forced Upper Ocean, M. F. Cronin and J. Sprintall

List of nomenclature, terms, and units used in the article:

Units:
Heat flux: W m^{-2}
Freshwater (precipitation-evaporation) flux: mm/day
Temperature: °C
Wind speed: m s^{-1}

Nomenclature:

τ : wins stress
τ_x: zonal component of the wind stress
τ_y: meridional component of the wind stress
W: wind speed
u: zonal component of the wind speed
v: meridional component of the wind speed
ρ: density of surface air
ρ_w: density of sea water
E: evaporation
Q_{LH}: latent heat flux
Q_{SH}: sensible heat flux
L_e: latent heat of vaporization
c_d: drag coefficient
c_e: turbulent exchange coefficient for latent heat
c_h: turbulent exchange coefficient for sensible heat
c_p: specific heat capacity of air at constant pressure
T_s: temperature at the sea surface
T_a: temperature at a reference height above the sea surface
q_s: specific humidity at the sea surface
q_a: specific humidity at a reference height above the sea surface

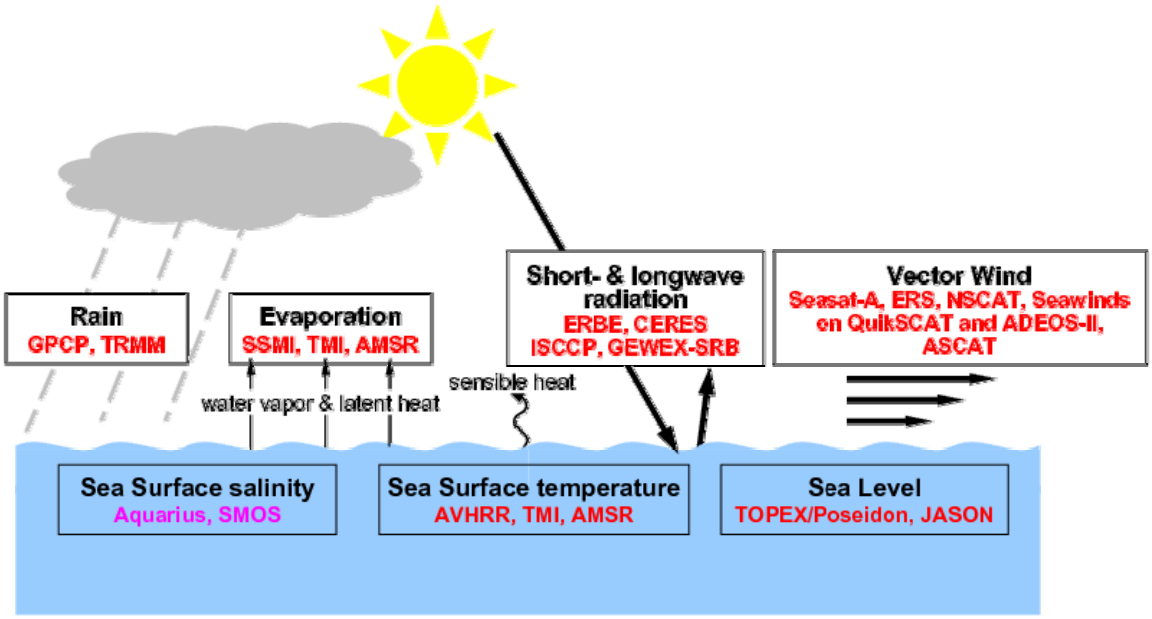
Rain
GPCP, TRMM
Evaporation
SSMI, TMI, AMSR
water vapor & latent heat
sensible heat
Short- & longwave radiation
ERBE, CERES
ISCCP, GEWEX-SRB
Vector Wind
Seasat-A, ERS, NSCAT, SeaWinds on QuikSCAT and ADEOS-II, ASCAT
Sea Surface salinity
Aquarius, SMOS
Sea Surface temperature
AVHRR, TMI, AMSR
Sea Level
TOPEX/Poseidon, JASON

Figure 1

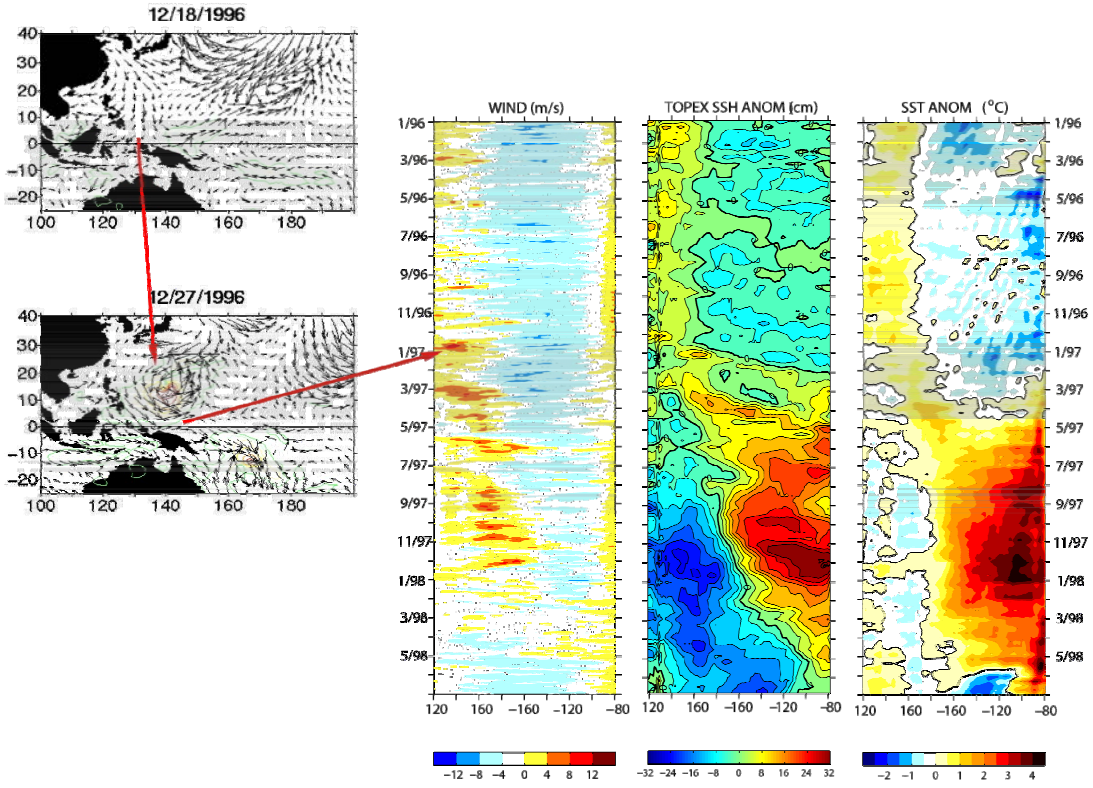

Figure 2

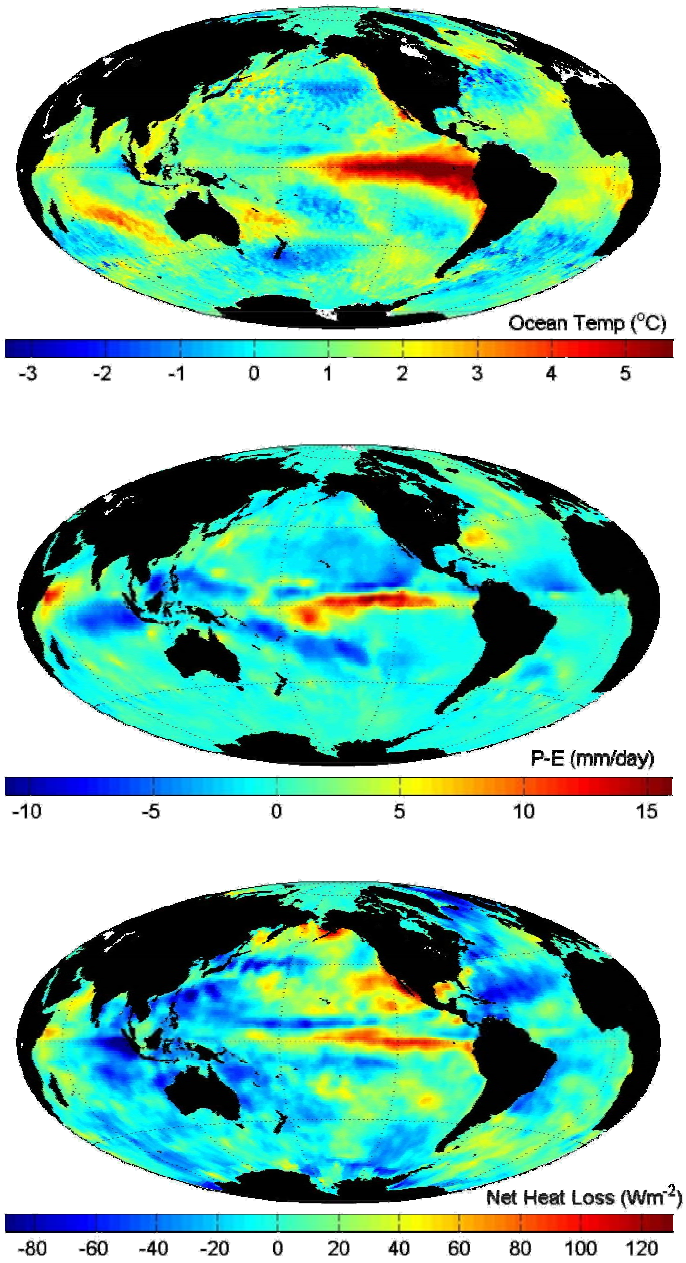
Ocean Temp (°C)
-3 -2 -1 0 1 2 3 4 5
P-E (mm/day)
-10 -5 0 5 10 15
Net Heat Loss (Wm-2)
-80 -60 -40 -20 0 20 40 60 80 100 120

Figure 3